Higher Order Bases in a 2D Hybrid BEM/FEM Formulation

Patrick W. Fink, *Member, IEEE*, and Donald R. Wilton, *Fellow, IEEE*

Abstract

The advantages of using higher order, interpolatory basis functions are examined in the analysis of transverse electric (TE) plane wave scattering by homogeneous, dielectric cylinders. A boundary-element/finite-element (BEM/FEM) hybrid formulation is employed in which the interior dielectric region is modeled with the vector Helmholtz equation, and a radiation boundary condition is supplied by an Electric Field Integral Equation (EFIE). An efficient method of handling the singular self-term arising in the EFIE is presented. The iterative solution of the partially dense system of equations is obtained using the Quasi-Minimal Residual (QMR) algorithm with an Incomplete LU Threshold (ILUT) preconditioner. Numerical results are shown for the case of an incident wave impinging upon a square dielectric cylinder. The convergence of the solution is shown versus the number of unknowns as a function of the completeness order of the basis functions.

Index Terms – BEM/FEM , Electromagnetic radiation and scattering, higher order, numerical analysis

I. Introduction

Two-dimensional, higher order basis functions have been shown to be advantageous both in FEM formulations and in integral equation formulations. Salazar-Palma, et. al., [1] examined higher order vector bases in various closed FEM problems. Hamilton, et.al., [2] examined higher order bases in TM scattering from a perfect electric conducting (PEC), circular cylinder. In each of these studies, the general observed trend was that increasing the completeness order of the basis functions improved the accuracy for a given number of unknowns, or reduced the number of unknowns required for a given accuracy. These benefits, however, are dependent upon the smoothness or regularity of the solution [1]. Prior to the common use of edge-based basis functions, Gong and Glisson [3] used linear and quadratic nodal basis functions in a 2D hybrid FEM/Method of Moments formulation. Later, Peterson, et. al., [4] employed higher order (quadratic for the TM case and linear for the TE case) scalar and vector bases in 2D scattering from heterogeneous objects with mesh termination provided by an absorbing boundary condition. It was shown that the increase from piecewise constant bases to piecewise

linear bases significantly improved the accuracy of the normal component at media interfaces.

The finite element method is often the preferred approach for modeling inhomogeneous or anisotropic regions. However, in unbounded regions, some method of terminating the finite-element mesh must be employed. Absorbing Boundary Conditions (ABC) and Perfectly Matched Layer (PML) absorbers have been used extensively to simulate an open boundary condition on the FEM mesh. While these methods preserve the sparsity of the system, they are not without drawbacks. In both, the mesh must extend away from the surface of the scattering object an acceptable distance, and some experimentation to determine this distance may be necessary. The use of the PML absorber results in poor conditioning of the resulting system [6], and material values for the component layers must be optimized over the band of interest. The ABC method involves higher order derivatives of the fields at the mesh termination. In addition, the ABC and PML are approximate boundary conditions. Since this work is intended for insertion into a production code (EIGER [7], [8]), we chose the BEM approach for mesh termination in order to minimize sources of error that might arise from a user's incomplete knowledge of the characteristics or limitations of the termination model.

In this paper, higher order basis functions are applied in the hybrid BEM/FEM formulation. The problem is formulated using the vector Helmholtz equation for the electric field in the homogenous, isotropic interior region. The fields on the exterior are represented in terms of equivalent electric and magnetic currents on the FEM region boundary, and a null field condition on the electric field just inside the boundary is used to obtain an Electric Field Integral Equation (EFIE) there [9]. It is shown that use of a generalized Gaussian quadrature is an accurate and efficient method for handling the singular self-term arising in the 2D EFIE. Numerical results are shown for a TE-polarized plane wave incident upon a square dielectric cylinder. Convergence of the equivalent electric and magnetic currents along the boundary is examined as a function of the completeness order of the basis functions. The Quasi-Minimal Residual (QMR) method with an Incomplete LU Threshold (ILUT) preconditioner is used to solve the resulting sparse system. The effects of the fill level and tolerance specified in the ILUT preconditioner are compared as the order of the basis function increases.

II. Problem Formulation

The problem addressed is TE plane wave scattering by a dielectric cylinder (Fig. 1). Each side of the cylinder is of length $d = 0.58\lambda_0$, where λ_0 is the wavelength in free space. The TE case was chosen since the operators involved have features similar to those encountered in the 3D case. The interior and exterior formulations are discussed in detail below, followed by a discussion on the enforcement of continuity of the tangential electric and magnetic fields at the interface.

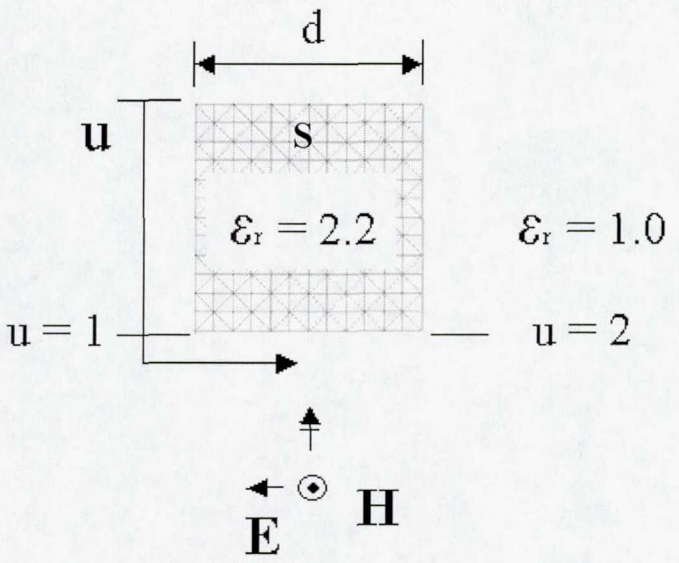

Figure 1. TE scattering from a square, dielectric cylinder.

A. Interior Formulation

The vector Helmholtz equation is used to model the electric field in the interior region,

$$\nabla \times \nabla \times \mathbf{E} - k^2 \mathbf{E} = -j\omega\mu \mathbf{J}, \tag{1}$$

where it has been assumed that the material is homogeneous and isotropic throughout the domain. It is also assumed that there are no impressed current sources inside the dielectric region, so the right-hand side of (1) vanishes. Curl-conforming, interpolatory basis functions are used to represent the electric field in the interior region:

$$\mathbf{E}(\boldsymbol{\rho}) \approx \sum_{j=1}^{N_E} V_j \, \boldsymbol{\Omega}_j^{(p)}(\boldsymbol{\rho}), \quad \boldsymbol{\rho} \in S, \tag{2}$$

where the superscript "p" denotes the completeness order of the basis, and N_E denotes the total number of unknowns associated with the interior electric field. The completeness order is the highest order such that all independent polynomial terms of that order or less are represented. The so-called "Whitney forms", or "edge bases", are used as the 0^{th} order basis functions. Basis functions of completeness order $p>0$ are obtained by multiplying the 0^{th} order edge basis function by a p^{th}-order *modified* or *shifted* Silvester interpolatory polynomial [10].

Equation (2) is inserted in (1), and the weak form of (1) is then obtained by the Galerkin method, resulting in

$$\sum_{j=1}^{N_E} V_j \left(\int_S \left(\nabla \times \mathbf{\Omega}_j^{(p)} \bullet \left(\nabla \times \mathbf{\Omega}_i^{(p)} \right) \right) dS' - k^2 \int_S \mathbf{\Omega}_j^{(p)} \bullet \mathbf{\Omega}_i^{(p)} \, dS' + \int_{\partial S} (\nabla \times \mathbf{\Omega}_j^{(p)}) \times \mathbf{\Omega}_i^{(p)} \bullet \hat{\mathbf{n}} \, d\ell \right) = 0, \quad \mathrm{i} = 1,..., \mathrm{N_e} , \tag{3}$$

where $\mathbf{\Omega}_i^{(p)}$ is the i$^{\text{th}}$ testing function, and $\mathbf{\Omega}_j^{(p)}$ is the j^{th} source basis function. The curl-curl term in (1) has been modified through the use of the divergence theorem, resulting in the first term of (3) and the introduction of a boundary integral term. This boundary integral term provides for coupling of the magnetic field to the exterior region through enforcement of the boundary condition on the tangential magnetic field. It can be thought of as providing the source for the FEM problem, as becomes more apparent when it is expressed in terms of the interior magnetic field at the boundary:

$$\sum_{j=1}^{N_E} V_j \left(\int_S \left(\nabla \times \mathbf{\Omega}_j^{(p)} \right) \bullet \left(\nabla \times \mathbf{\Omega}_i^{(p)} \right) dS' - k^2 \int_S \mathbf{\Omega}_j^{(p)} \bullet \mathbf{\Omega}_i^{(p)} \, dS' \right) = j\omega\mu \int_{\partial S} (\hat{\mathbf{n}} \times \mathbf{H}) \bullet \mathbf{\Omega}_i^{(p)} \, d\ell, \quad \mathrm{i} = 1,..., \mathrm{N_e} \tag{4}$$

Note that the basis function for the tangential magnetic field is identical to that used for the electric current in the exterior formulation. This is discussed in more detail below.

B. Exterior Formulation

The exterior region is modeled using the Electric Field Integral Equation (EFIE). Using the equivalence principle, electric and magnetic currents are placed around the boundary of the cylinder, and the total tangential electric field is set equal to zero just inside the boundary:

$$\frac{\mathbf{M}}{2} - \hat{\mathbf{n}} \times \left(j\omega \mathbf{A} + \nabla\Phi + \frac{1}{\varepsilon} \nabla \times \mathbf{F} \right) + \hat{\mathbf{n}} \times \mathbf{E}_{inc} = 0, \quad \boldsymbol{\rho} \uparrow \partial S \tag{5}$$

Here, $\mathbf{E}_{inc}$ is the electric field associated with the incident plane wave in the absence of the scattering object, $\hat{\mathbf{n}}$ is the normal to the contour, and the "$\uparrow$" implies that the bounding contour is approached from the inside. The jump discontinuity of the curl term caused by the magnetic current $\mathbf{M}$ has been removed and presented explicitly in the first term. Therefore, the electric field at the observation point $\boldsymbol{\rho}$ due to the curl term arises only from the magnetic current away from point $\boldsymbol{\rho}$ [11]. Furthermore, all current, field, and potential dependence upon the position, $\boldsymbol{\rho}$, on the cylinder has been suppressed for notational simplicity. Since the sources are radiating in a homogeneous region, the potentials can be expressed using the free-space Green's function, $G(\boldsymbol{\rho}, \boldsymbol{\rho}')$, and (5) becomes

$$\frac{\mathbf{M}(\boldsymbol{\rho})}{2} - \hat{\mathbf{n}} \times \left(j\omega\mu \int_{\partial S} \mathbf{J}(\boldsymbol{\rho}') G(\boldsymbol{\rho}, \boldsymbol{\rho}') \, d\ell' - \frac{1}{j\omega\varepsilon} \nabla \int_{\partial S} \nabla' \cdot \mathbf{J}(\boldsymbol{\rho}') G(\boldsymbol{\rho}, \boldsymbol{\rho}') \, d\ell' + \right.$$
$$\left. \nabla \times \int_{\partial S_0} \mathbf{M}(\boldsymbol{\rho}') G(\boldsymbol{\rho}, \boldsymbol{\rho}') \, d\ell' \right) = -\hat{\mathbf{n}} \times \mathbf{E}_{inc}(\boldsymbol{\rho}), \quad \boldsymbol{\rho} \in \partial S, \tag{6}$$

where ∂S_0 indicates that the integral does not contribute at $\boldsymbol{\rho}' = \boldsymbol{\rho}$, and the prime notation indicates source point coordinates.

On the boundary segments, piecewise polynomial, interpolatory basis functions are used to represent the magnetic currents, which are z-directed in the TE formulation:

$$\mathbf{M}(\boldsymbol{\rho}) \approx \hat{\mathbf{z}} \sum_{j=1}^{N_M} \tilde{V}_j \, \Pi_j^{(p)}(\boldsymbol{\rho}), \quad \boldsymbol{\rho} \in \partial S, \tag{7}$$

where N_M is the total number of unknowns associated with the magnetic current, and the superscript "p" is again the order of polynomial completeness. $\tilde{V}_j$ denotes the coefficients of the magnetic current, which constitute a subset of the coefficients, V_j, of the electric field (2) as discussed below. $\Pi^{(p)}(\boldsymbol{\rho})$ is simply the product of the p^{th}-order modified Sylvester polynomial that interpolates the j^{th} unknown and a pulse function that is unity when $\boldsymbol{\rho}$ is within the support of the segment, and zero otherwise. This choice of basis function allows for straightforward enforcement of tangential continuity across the boundary, ∂S, as discussed below.

The electric currents are also represented by piecewise polynomial, interpolatory basis functions [10]:

$$\mathbf{J}(\boldsymbol{\rho}) \approx \sum_{j=1}^{N_J} I_j \, \boldsymbol{\Lambda}_j^{(p)}(\boldsymbol{\rho}), \qquad \boldsymbol{\rho} \in \partial S \tag{8}$$

$$\text{with } \boldsymbol{\Lambda}_j^{(p)} = \hat{\ell}_j \, \Lambda_j^{(p)}(\boldsymbol{\rho}),$$

where $\hat{\ell}_j$ is the unit vector along the j^{th} segment, and $\Lambda_j^{(p)}(\boldsymbol{\rho})$ is the p^{th}-order, interpolatory scalar function that interpolates the j^{th} node in the set of N_J degrees of freedom associated with the electric currents. It should be noted that electric current bases for interpolation points that coincide with segment endpoints span the support of the contiguous segments in order to ensure continuity of current across the segments. Bases that interpolate interior points have only a single segment as their support. While this choice of basis function provides a differentiable function within the element and ensures current continuity between segments, it also implies that the lowest completeness order for the electric current is $p = 1$. This is in contrast to the basis representations for the electric field and equivalent magnetic current, where the lowest order is p=0.

As in the interior formulation, the Galerkin choice for testing functions is used to obtain the weak form of (6) by dot multiplying both sides by $\Lambda_{\mathrm{m}}^{(\mathrm{p})}$, yielding

$$\sum_{j=1}^{N_M} \tilde{V}_j \int_{\partial S_m} \left[(\Lambda_{\mathrm{m}}^{(\mathrm{p})} \times \hat{\mathbf{n}}) \bullet \frac{\hat{\mathbf{z}}\, \Pi_j^{(p)}(\boldsymbol{\rho})}{2} + \Lambda_{\mathrm{m}}^{(\mathrm{p})} \bullet \left(\nabla \times \int_{\partial S_0} \hat{\mathbf{z}}\, \Pi_j^{(p)}(\boldsymbol{\rho}')\, \mathrm{G}(\boldsymbol{\rho},\boldsymbol{\rho}')\, \mathrm{d}\ell' \right) \right] d\ell$$

$$+ \sum_{k=1}^{N_J} I_k \int_{\partial S_m} \left[\Lambda_{\mathrm{m}}^{(\mathrm{p})} \bullet \mathrm{j}\omega\mu \int_{\partial S_k} \Lambda_{\mathrm{k}}^{(\mathrm{p})}(\boldsymbol{\rho}')\, \mathrm{G}(\boldsymbol{\rho},\boldsymbol{\rho}')\, \mathrm{d}\ell' + \right.$$

$$\left. \frac{1}{\mathrm{j}\omega\varepsilon} (\nabla \bullet \Lambda_{\mathrm{m}}^{(\mathrm{p})}) \int_{\partial S_k} \nabla' \bullet \Lambda_{\mathrm{k}}^{(\mathrm{p})}(\boldsymbol{\rho}')\, \mathrm{G}(\boldsymbol{\rho},\boldsymbol{\rho}')\, \mathrm{d}\ell' \right] d\ell \qquad (9)$$

$$= \int_{\partial S_m} \Lambda_{\mathrm{m}}^{(\mathrm{p})} \bullet \mathbf{E}_{\mathbf{inc}}(\mathbf{r})\, d\ell, \qquad \boldsymbol{\rho} \in \partial S, \quad m = 1, \ldots N_J \ ,$$

where an integration by parts and the divergence theorem are used to transfer derivatives from the scalar potential onto the testing function. The number of testing functions in (9) corresponds to the number of electric current unknowns, N_J. This is a result of the strong continuity enforcement in which the degrees of freedom associated with the magnetic current are shared with the electric field along the boundary of the interior FEM region. Thus, the set of unknowns corresponding to the magnetic field, $\{\tilde{V}_M\}$, is a subset of the total set of unknowns for the electric field, $\{V_E\}$.

C. Accurate Integration of Self-Term

In order to realize the expected improvements in accuracy afforded by the higher order bases, it is necessary to accurately integrate all matrix entries; this requires that special consideration be given to the integration of singular self-terms.

In two dimensions, the Green's function in (9) is given by [11]

$$G(\boldsymbol{\rho}, \boldsymbol{\rho}') = \frac{H_0^{(2)}(kD)}{4j}, \qquad (10)$$

where $D \equiv |\boldsymbol{\rho} - \boldsymbol{\rho}'|$. As the source point, $\boldsymbol{\rho}'$, approaches the observation point, $\boldsymbol{\rho}$, the Hankel function may be approximated by [12]:

$$H_0^{(2)}(kD) \approx 1 - j\frac{2}{\pi} \ln\left(\frac{\gamma\, k D}{2}\right), \qquad (11)$$

where $\ln\gamma$ is Euler's constant (0.5772...). To accurately integrate the logarithmic singularity, the generalized Gaussian quadrature rule introduced by Ma et. al., [13] is used. This rule exactly integrates linear combinations of the functions

$$1,\ \ln(x), x, x\ln(x),\ x^2,\ x^2\ln(x),\ \ldots\ x^{N-1}\ln(x) \tag{12}$$

on the interval (0,1) with an N-point rule. To implement this quadrature rule, the source segment is simply divided into two subsegments on either side of the observation point and each is reparameterized with the parameter origin at the observation point where the Green's function is singular.

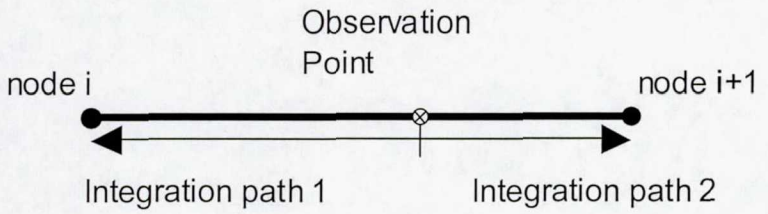

Figure 2. Integration using generalized quadrature rule.

D. Continuity Enforcement

To uniquely determine the fields in the exterior and interior regions, continuity of the tangential fields at the boundary must be enforced in some sense. As a result of the interpolatory basis functions selected for the interior electric field and the exterior magnetic current, the nodes associated with each are collocated along the boundary, ∂S. Since it is the tangential component of the interior electric field that is interpolated at these boundary nodes, and the magnetic current is $\hat{\mathbf{z}}$-directed, assigning a single degree of freedom for each pair of collocated nodes for **E** and **M** enforces strong tangential continuity of the electric field across the boundary. Similarly, the same basis function and degree of freedom used to model the electric current on the exterior is also used to represent the tangential magnetic field in (4).

E. Matrix Structure and Sparse Solver

The linear system of equations consists of a total of N_J densely populated rows corresponding to the EFIE (9) and N_E sparsely populated rows corresponding to the Helmholtz equation (4). This system was solved by direct LU decomposition for the smaller problems considered. For larger problems, memory and speed considerations necessitate the use of an iterative method. Without any type of matrix normalization, the

hybrid system is very ill-conditioned. Therefore, column scaling was used prior to the iterative solution process [14]. The Quasi-Minimal Residual (QMR) iterative method was then employed with an Incomplete LU Threshold (ILUT) preconditioner [15]. This preconditioner approximates the complete LU factorization as

$$LU \approx A = \hat{L}\hat{U}, \tag{13}$$

where A is the system matrix formed from (9) and (4), and L and U are obtained by applying a sparsity pattern to the standard $\hat{L}\hat{U}$ factorization. For each row in L and U, the sparsity pattern may be affected by two parameters, a fill-in factor, *fill_limit*, and a tolerance factor, *TOL*. The fill-in factor specifies the maximum number of entries, in addition to the number of non-zero row entries of the original matrix, to be allowed in the corresponding rows of L and U. Only the largest *fill_limit* entries in a row of L or U are retained, and these sets are denoted by $S_i^{(L)}$ and $S_i^{(U)}$, respectively, for the i^{th} row. The final sparsity pattern is then determined dynamically for each row of L and U by disallowing any positions in $S_i^{(L)}$ and $S_i^{(U)}$ for which the corresponding value is less than a specified tolerance. This tolerance is computed as the product of the average magnitude of the row entries and the user specified tolerance factor, *TOL*. The tolerance criterion for the matrix element to be included in the sparsity pattern of L is summarized by

$$\left|\ell_{ij}\right| \geq \frac{TOL}{N_{zi}^{(L)}} \times \sum_{m=1}^{N_{zi}^{(L)}} \left|\ell_{im}\right|, \quad j \in S_i^{(L)}, \tag{14}$$

where ℓ_{ij} is the (i,j) entry in the matrix L, TOL is the user-specified tolerance, and $N_{zi}^{(L)}$ is the total number of non-zero elements in the lower part (i.e., $j < i$) of the i^{th} row. A similar condition exists for entries of U.

III. Numerical Results

A. Eigenvalues of a Square Conducting Cylinder

In order to verify the functionality of the finite-element formulation and code, the generalized eigenvalues, k^2 in (1), were computed for the case of a square, cylindrical conducting cavity with an interior relative permittivity of $\varepsilon_r = 1.0$. For this case, the relative permittivity was set to unity. The theoretical convergence rate for the eigenvalues is [1]

$$\left|\lambda_i - \tilde{\lambda}_i\right| \leq C h^{2(p+1)}, \tag{15}$$

where h is the extent of the element, λ_i is the numerically obtained estimate of the i^{th} eigenvalue, $\tilde{\lambda}_i$ is the i^{th} exact eigenvalue, p is the order of polynomial completeness, and C is a constant that depends on the element type, but is independent of h. Figure 3 shows

the convergence versus the number of segments for basis completeness orders ranging from one to five. The slopes for the theoretical rates of convergence are shown for comparison in the lower left corner where $s = 2(p+1)$. The convergence rates compare favorably with the theoretical rates. The p =5 curve appears to converge faster than the theoretical rate; however, the two data points obtained for this case are probably insufficient to reveal the final convergence rate.

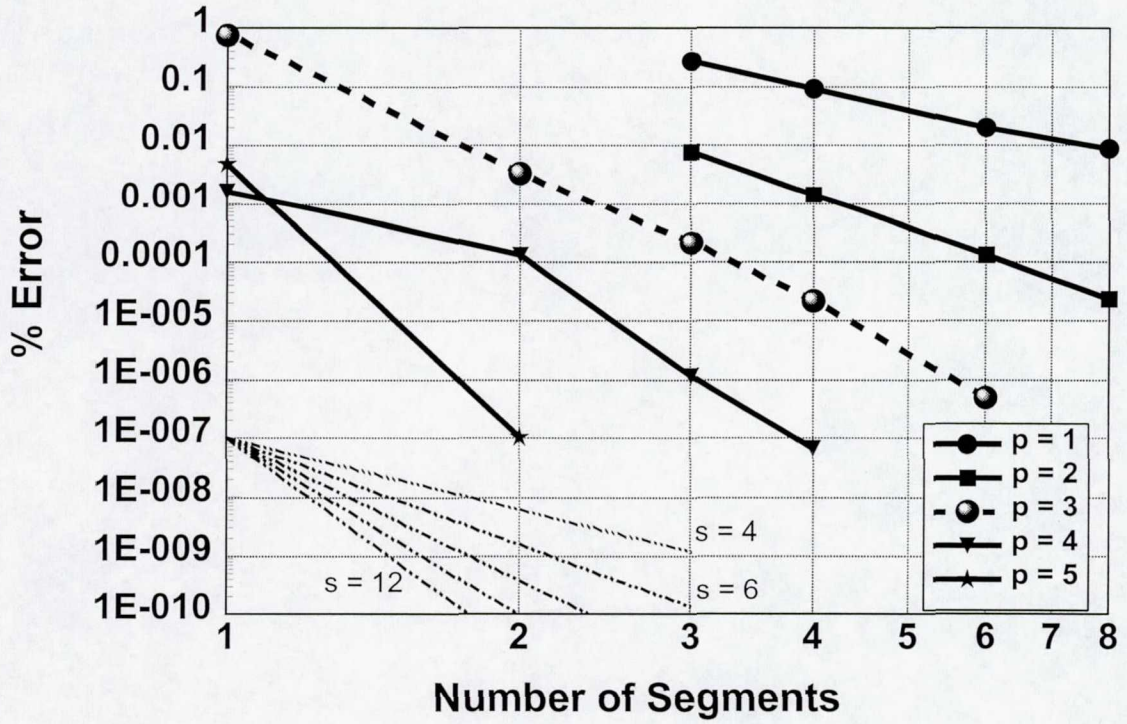

Figure 3. Convergence of lowest eigenvalue for a square cylinder with bases of completeness order p on triangular elements.

B. Dielectric Cylinder

In this section, results are presented for the case of TE plane wave scattering by a square, dielectric cylinder. The relative permittivity of the cylinder is $\varepsilon_r = 2.2$, and the length of each side of the square is $0.58\ \lambda_0$. In Fig. 4, the equivalent electric current is plotted as a function of the normalized distance around the square (Fig. 1), where the normalized side length is unity. The basis order p is the completeness order for the electric current bases. In the case p=5, the entire finite element region comprises just two triangles. It can be seen that the p=5 case with just 85 unknowns compares very well with the p=1 baseline case with 15,000 unknowns.

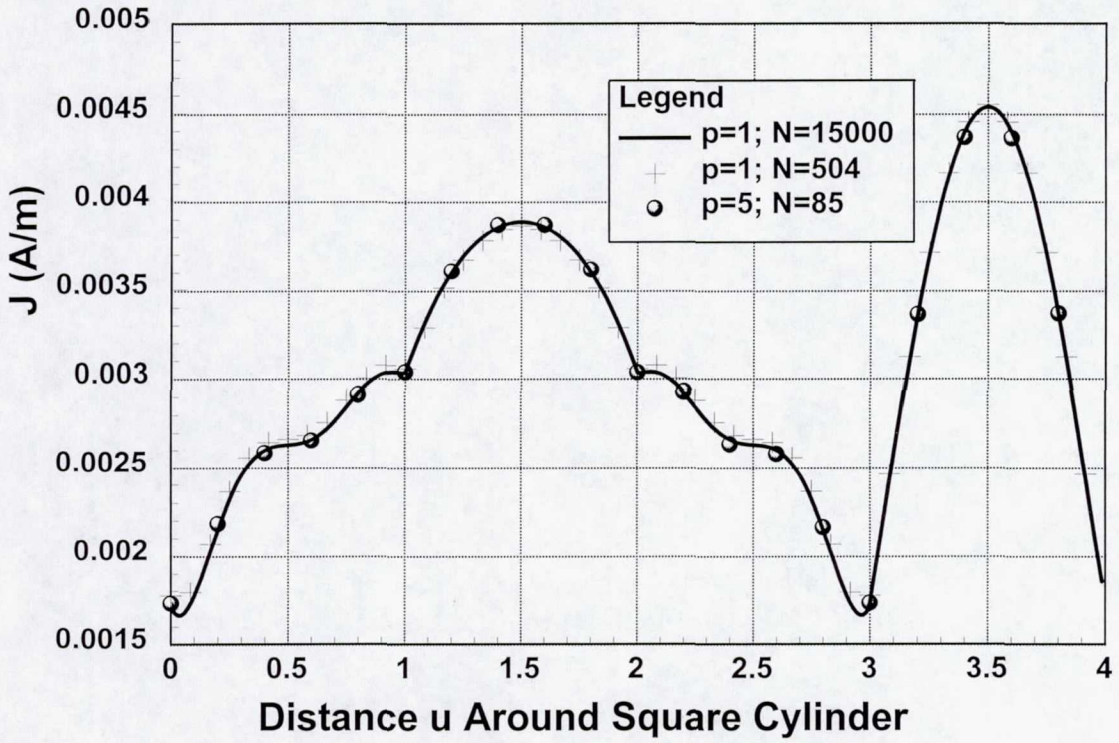

Figure 4. Equivalent electric current on a square, dielectric cylinder.

Figure 5 is a similar plot of the equivalent magnetic current along the boundary. In this graph, p is the completeness order of the magnetic current bases. Note that both the p=0 and p=4 solutions appear close to the baseline over much of the plot. However, the p=0 case has nodes nearer the vertices where the magnetic current is singular, and the error is significant at these points.

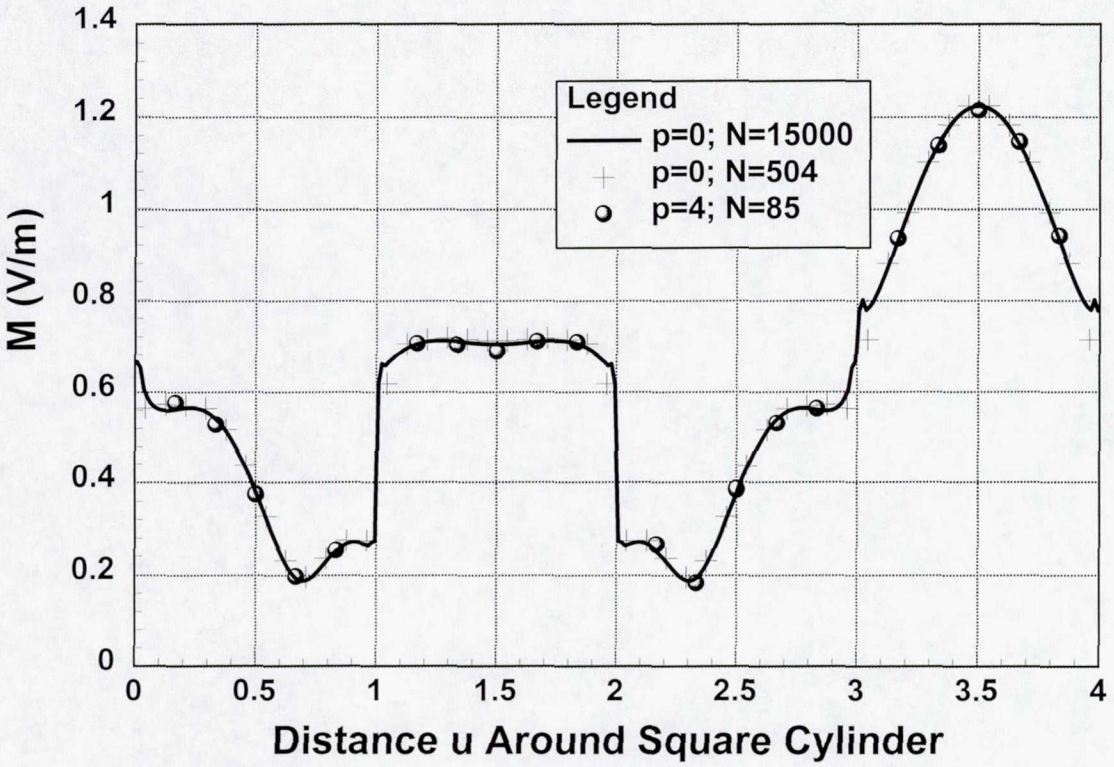

Figure 5. Equivalent magnetic current on a square, dielectric cylinder.

Figure 6 shows the convergence of the equivalent electric current as a function of the completeness order of the electric current bases. The result obtained from a p=1 solution with 15,000 unknowns was used as the baseline. For comparison, curves showing the rates of convergence,

$$N^{-\alpha/2}\ ,\ \alpha = 1,\ldots 5$$
$$s = \alpha/2\ , \tag{16}$$

where N is the number of unknowns, are inset in the lower left corner of Fig. 6. These rates correspond to the convergence of a closed domain, FEM solution with different orders of polynomial approximation, α, when the local errors are of the same order of magnitude [1]. Since the elements in this study were of uniform length, and the error will most likely be greater near the cylinder corners, this latter condition is certainly violated. Nonetheless, there is a dramatic improvement in convergence of the p=2 case compared to p=1. The p=3 case shows marginal improvement over p=2, and orders higher than p=3

do not appear to offer convergence benefits for the electric current in this problem. It should be noted that, due to the edge singularity in the magnetic current, the higher order bases are probably disadvantageous near the corners of the cylinder. This edge singularity likely causes a diminishing return in accuracy with higher basis orders for this problem.

Figure 7 shows a similar convergence plot for the equivalent magnetic current as a function of the completeness order of the magnetic current bases. As in Fig. 6, curves showing rates of convergence that correspond to the same closed domain problem described above are inset in the lower left corner for comparison. As was the case with the electric current, the error in the magnetic current is almost certainly not uniform across the elements, but it can be seen that the slopes for the cases $p = 1$, 2, and 3 agree well with the inset curves prior to leveling off. Furthermore, Fig. 7 reveals that there is a significant advantage associated with the use of higher order bases up to $p = 3$ or 4, even though the convergence rates are not sustained as the nodes approach corners. Comparing Figs. 6 and 7, there is a more pronounced improvement with basis order for the magnetic current than for the electric current. This may be due, in part, to the fact that the increase in unknowns for the trials associated with lower basis orders results in more nodes near the corner where the magnetic current is singular. However, there is a noticeable decrease in the slope of all curves for which $p > 0$, and this also is due to the inability of the smoother basis functions to model the singularity near the corners. This is revealed in Fig. 8, which shows a distribution of the error for two trials with p=2. As the number of unknowns increase from 408 to 1488, it can be seen that the convergence near the corners is very poor.

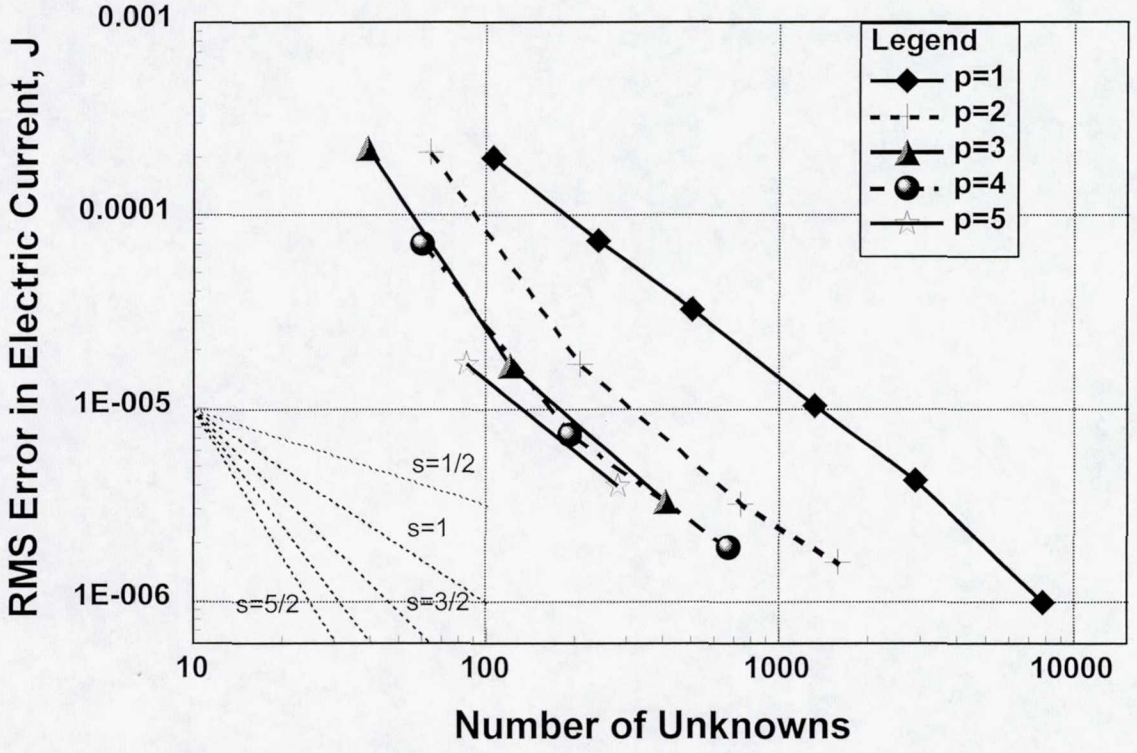

Figure 6. Convergence of equivalent electric current, $\mathbf{J}$, as a function of basis order.

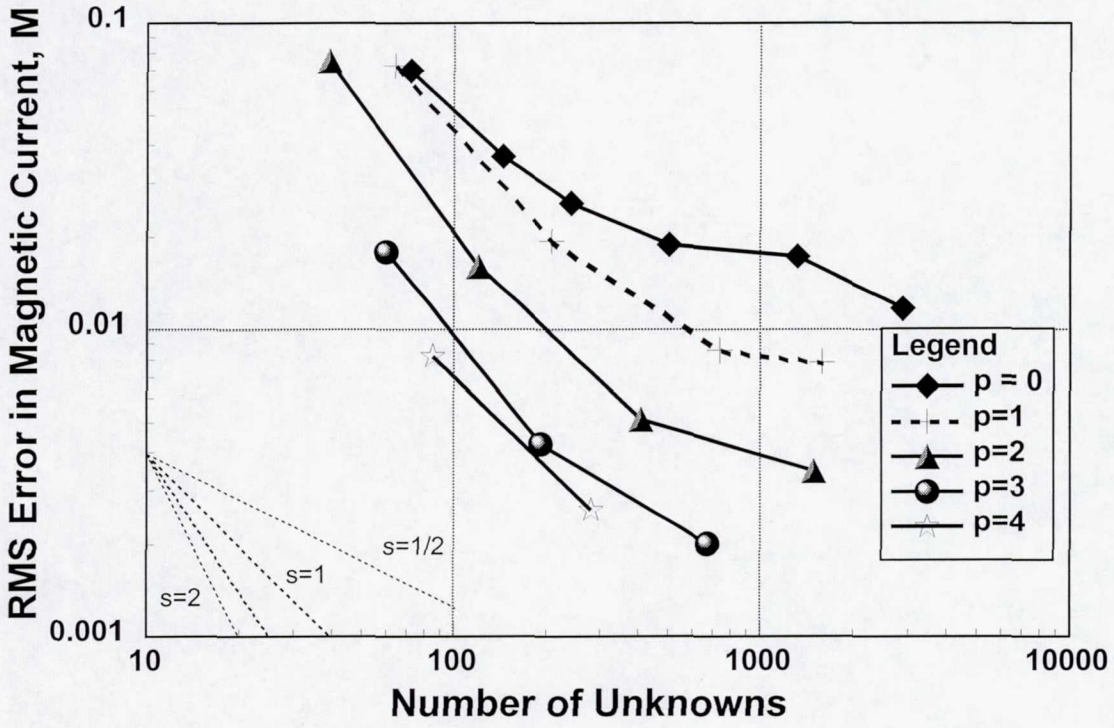

Figure 7. Convergence of equivalent magnetic current, M, as a function of basis order.

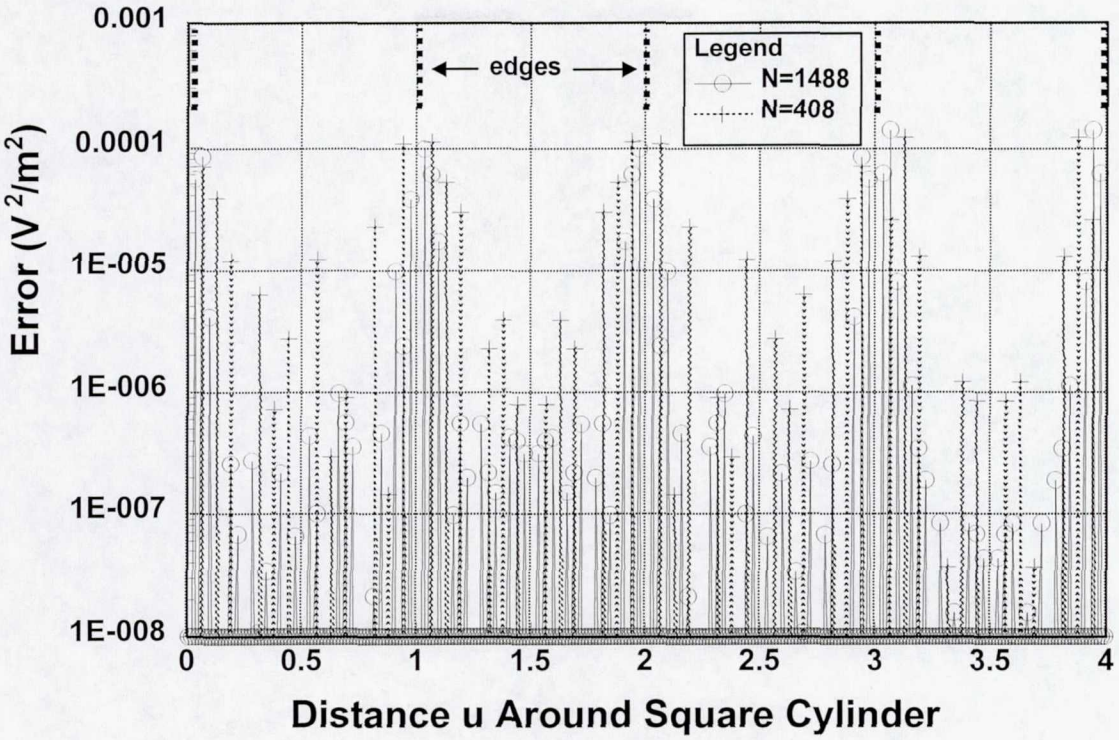

Figure 8. Distribution of error as a function of u for two trials with p=2.

C. Iterative Solver

For the numerical convergence results discussed above, all of the problems except the baseline could be readily solved via direct Gaussian elimination. However, various trials were run to investigate the suitability of the Quasi-Minimal Residual (QMR) iterative solver with an Incomplete LU Threshold (ILUT) preconditioner for the hybrid system defined by (4) and (9). The trials consisted of different values for the tolerance and maximum fill-in parameters for the ILUT preconditioner. In all trials, a column-norm scaling was implemented prior to the iterative solution process.

It was found that there existed narrow ranges of the tolerance and fill-in parameters that permitted stable operation of the iterative solver with the resulting preconditioner. Table 1 below shows the two input parameters, tolerance, *TOL*, and fill-in factor, *fill_limit*, as well as the number of nonzero entries in the resulting L and U matrices for a p=0 case with 2,880 unknowns. The first row corresponds to a complete fill-in, and, hence, is equivalent to a sparse direct solve method. The second to last column shows the cumulative number of nonzero entries in L and U as a percentage of the total number of non-zero entries required for a sparse direct solution (*fill_limit* =100% and *TOL*=0). In the final column, the convergence results are stated as the number of two-term QMR iterations required for an absolute residual of less than 10^{-6}. It should be noted that cases

in which the preconditioner failed were marked by excessively large norms of the initial residual after the first approximate inverse.

It can be seen from Table 1 that, for the case of p=0 with 2880 unknowns, the resulting size of the preconditioner is approximately 75% of the complete fill-in required for a sparse direct solution. Table 2 contains results for a p=3 case with 2496 unknowns. As expected, the p=3 matrix is not as sparse as the p=0 matrix. In addition, the resulting size of the preconditioner, approximately 85% of the full fill-in from a direct solver, is larger than that achieved for the p=0 case. In [5] it was found that quadratic and linear bases resulted in similar fill-in for a nearly equal number of unknowns. In contrast, a marked increase in fill-in for the p=3 case can be seen in trial 1 of Table 2 compared to trial 1 in Table 1. It should be noted that, in the cases presented here, no re-ordering of the system matrix was attempted.

Two additional trials were run for the case p=0 with 15,000 unknowns. These results are shown in Table 3, where it can be seen that the resulting ILUT preconditioner is about 70% of the size of the complete, sparse LU factorization.

Table 1. Trials with p=0, N = 2880 unknowns.

Trial	*TOL*	*fill_limit* (%)	L	U	(L+U) (%)	Iterations
1	0	100.	306,870	299,877	100.0	1
2	0	10.	169,661	299,877	77.4	10
3	0	5.	157,061	299,877	75.3	15
4	0	4	153,945	292,408	73.6	22
5	0	3	147,951	246,512	65.0	failed
6	0.0025	100.	296,486	298,339	98.0	5
7	0.01	100.	270,195	293,339	92.9	9
8	0.05	100.	168,767	269,262	72.2	69
9	0.075	100.	131,146	253,211	63.3	failed
10	0.01	10.	154,354	293,339	73.8	17
11	0.02	10.	135,629	286,760	69.6	failed

Table 2. Trials with p=3, N = 2496 unknowns.

Trial	*TOL*	*fill_limit* (%)	L	U	(L+U) (%)	Iterations
1	0	100.	503,396	495,692	100.0	1
2	0	15.	388,212	495,692	88.5	12
3	0	10.	354,744	495,692	85.1	16
4	0	7.5	286,316	453,016	74.0	failed
5	0.0025	100.	412,582	486,011	89.9	16
6	0.005	100.	368,128	478,775	84.8	37
7	0.0075	100.	309,825	467,131	77.8	failed
8	0.001	10.	335,273	491,409	82.7	31
9	0.05	10.	148,974	435,175	58.5	failed

Table 3. Trials with p=0, N = 15,000 unknowns.

Trial	*TOL*	*fill_limit* (%)	L	U	(L+U) (%)	Iterations
1	0	100.	3728130	3689417	100.0	1
2	0.005	10.	1647754	3551338	70.1	21

III. Conclusions

A FEM/BEM formulation using higher order, interpolatory vector basis functions was presented for application to TE scattering from dielectric cylinders. A similar formulation including results for scattering by 3D objects will be reported in the near future. Although the formulation was applied to a homogeneous cylinder, it can be readily adapted to inhomogeneous cylinders as well. A generalized Gaussian quadrature [13] was implemented and found to provide accurate and efficient integration of the singular self-terms.

In order to verify the FEM code, the convergence of the lowest eigenvalue of a square conducting cylinder was examined as a function of mesh density (h-refinements) and of basis completeness order (p-refinements). Numerical results were presented for the case of a TE plane wave impinging upon a dielectric square cylinder. The equivalent electric and magnetic boundary currents were plotted for the cases of low (p=0 for the magnetic currents) and high (p=4 for the magnetic currents) basis completeness orders. Finally, h-p convergence was examined for the equivalent boundary currents with a 15,000 unknown p=0 (magnetic current) solution serving as a baseline. For both the electric and magnetic equivalent currents, the use of higher order bases improved the convergence significantly up to order p=3. The convergence rates tended to subside, however, beyond a certain level of h-refinement. It is suspected that this is due to the edge singularity of the magnetic current. Near edges, achieving full advantage from the use of higher order basis functions will likely require equilibrated meshes [1] or the use of singular basis functions [16].

An ILUT preconditioner, used in conjunction with QMR, was shown to provide solutions with very few iterations, but provided only modest reductions in the required memory when compared to a complete, sparse LU factorization. Adjusting the tolerance and fill-in parameters for the implemented ILUT preconditioner did not permit a reduction of fill-in at the expense of QMR iterations. Rather, there appeared to be a distinct threshold below which the preconditioner provided a very good approximation to the inverse of the original system, but above which the preconditioner became very poorly conditioned. The ILUTP method, in which the "P" stands for pivoting, is recommended in [14] as a remedy for unstable results with the ILUT preconditioner, but has not been applied in this study.

References

[1] Salazar-Palma, M., et. al., *Iterative and Self-Adaptive Finite-Elements in Electromagnetic Modeling*. Boston: Artech House, 1998.

[2] Hamilton, L.R., et. al., "Method of Moments Scattering Computations Using High-Order Basis Functions," *Antennas and Propagation Society International Symposium*, IEEE, 1993 Digest, vol. 3, pp1132-1135.

[3] Gong, Z., Glisson, A., "A Hybrid Equation Approach for the Solution of Electromagnetic Scattering Problems Involving Two-Dimensional Inhomogeneous Dielectric Cylinders," *IEEE Trans. Antennas Propagat.,* vol. 38, pp. 60-68, Jan. 1990.

[4] Peterson, A.F., Scott, L.R., Mittra, R., *Computational Methods for Electromagnetics*, New York: IEEE Press, 1998.

[5] Peterson, A.F., "Vector Finite Element Formulation for Scattering from Two-Dimensional Heterogeneous Bodies," *IEEE Trans. Antennas Propagat.,* vol. 43, pp. 357-365, Mar. 1994.

[6] Botros, Y., and Volakis, J., "A Robust Iterative Scheme for FEM Applications Terminated by the Perfectly Matched Layer (PML) Absorbers," *15th National Radio Science Conference (URSI)*, Cairo, Egypt, 1998.

[7] W. A. Johnson, R. E. Jorgenson, L. K. Warne, J. D. Kotulski, J. B. Grant, R. M. Sharpe, N. J. Champagne, D. R. Wilton, and D. J. Jackson, , "Our experiences with object oriented design, FORTRAN 90, and massively parallel computations" 1998 Digest USNC/URSI National Radio Science Meeting, June 21 - 26, 1998, Atlanta, Georgia, Antennas: Gateways to the Global Network, p. 308.

[8] Sharpe, R.M., et. al., "EIGER: Electromagnetic Interactions GEneRalized," *Antennas and Propagation Society International Symposium, IEEE*, 1997 Digest, vol. 4.

[9] Volakis, J.L., Chatterjee, A., and Kempel, L.C., *Finite Element Method for Electromagnetics*, New York: IEEE Press, 1998.

[10] Graglia, G.D., Wilton, D.R., and Peterson, A.F., "Higher Order Interpolatory Vector Bases for Computational Electromagnetics," *IEEE Trans. Antennas Propagat.*, vol. AP-45, no. 3, pp. 329-342, March 1997.

[11] Wilton, D.R., "Computational Methods," chapter in *Scattering,* R.Pike and P. Sabatier, Eds., London: Academic Press, 2002.

[12] Harrington, R.F., *Time-Harmonic Electromagnetic Fields*, New York: McGraw-Hill, 1987.

[13] Ma, J., Rokhlin, V., Wandzura, S., "Generalized Gaussian Quadrature Rules for Systems of Arbitrary Functions," *SIAM J. Numer. Anal.*, vol. 33, no. 3, pp. 971-996, June 1996.

[14] Saad, Yousef, *Iterative Methods for Sparse Linear Systems*, Boston: PWS Publishing Co., 1996.

[15] Freund, R.W., Nachtigal, N.M.," An Implementation of the QMR Method Based on Coupled Two-Term Recurrences," *SIAM Journal on Scientific Computing*, vol 15, pp. 313—337, 1994.

[16] Brown, W., Wilton, D.R., "Singular Basis Functions and Curvilinear Triangles in the Solution of the Electric Field Integral Equation," *IEEE Trans. Antennas Propagat.*, vol. AP-47, no. 2, pp. 347-353, Feb. 1999.

[17] Pantic-Tanner, Z., et. al., "Two-Dimensional Singular Vector Elements for Finite-Element Analysis," *IEEE Trans. Antennas Propagat.*, vol. 46, no. 2, pp. 178-184, Feb. 1998.